# An efficient synthesis and characterization of La@MOF-808: A promising strategy for effective arsenic ion removal from water

Hassan Nawaz [a,b], Muhammad Ibrahim [a,*], Abid Mahmood [a], Gregg P. Kotchey [b], David V.P. Sanchez [b,c,**]

[a] *Department of Environmental Sciences, Government College University Faisalabad, Pakistan*
[b] *Department of Civil and Environmental Engineering, Swanson School of Engineering, University of Pittsburgh, Pittsburgh, PA, 15261, United States*
[c] *Mascaro Center for Sustainable Innovation, Swanson School of Engineering, University of Pittsburgh, Pittsburgh, PA, 15261, United States*

ARTICLE INFO

ABSTRACT

Addressing serious waterborne arsenic issues, for the first time, lanthanum-doped MOF-808 (La@MOF-808) has been developed to remove total arsenic (Total As) and arsenite [As(III)] from water. This study involves the solvothermal synthesis of La@MOF-808, its characterization via FTIR, XRD, TGA, and SEM, in which distinct physicochemical attributes were identified, and the adsorption capacity of arsenic ions. The saturated adsorption capacity of La@MOF-808 for Total As and As(III) reached 282.9 mg g$^{-1}$ and 283.5 mg g$^{-1}$, as compared to 229.7 mg g$^{-1}$ and 239.1 mg g$^{-1}$ for pristine MOF-808, respectively. XRD and ATR-FTIR analyses underscored the central roles of electrostatic interactions and hydroxyl groups in the pollutant adsorption process. The impact of temperature, concentration, pH, and exposure duration times on adsorption performance was thoroughly investigated. The Langmuir model showed the maximum adsorption capacities ($q_{max}$) of La@MOF-808 was 307.7 mg g$^{-1}$ for Total As and 325.7 mg g$^{-1}$ for As(III), surpassing those of MOF-808 adsorbent, which suggests that monolayer adsorption occurred. Optimal adsorption was observed in a pH range of 2.0–7.0, and thermodynamic studies classified the process as spontaneous and endothermic. The adsorbent retains high capacity across repeated cycles, outperforming many standard adsorbents. Lanthanum doping markedly enhances MOF-808's arsenic removal, underscoring its potential for water treatment.

## 1. Introduction

Metal-Organic Frameworks (MOFs) are complex and highly structured three-dimensional lattice assemblies comprised of repetitive, interconnected chemical units known as secondary building units (SBUs) [1]. SBUs consist of metal ions or clusters that are chemically coordinated with organic ligands or molecules. The selection of metal ions and organic molecules for the SBUs, coupled with the method of synthesis, yields unique physicochemical attributes like porosity, surface area, and reactivity [1].

Over the past few decades, the convergence of inorganic chemistry and materials science has produced a systematic understanding of MOF chemistry resulting in the capacity to intelligently design these materials [2]. Consequently, from 1995 to 2002, around 6000

**Abbreviations**

Total As   Total Arsenic (1:1 ratio of sodium arsenate and arsenite)
As (III)   Arsenite
ATR- FTIR   Attenuated Total Reflectance - Fourier Transform Infrared Spectroscopy
TGA   Thermogravimetric Analysis
XRD   X- Ray Diffraction
SEM   Scanning Electron Microscope
La@MOF-808   Lanthanum doped- Metal Organic Framework-808

distinct MOF structures have been discovered and documented [1]. Subsequently, from 2003 to 2009, the introduction of reticular chemistry opened new possibilities, resulting in the synthesis of a wide range of MOF materials with diverse pore geometries and characteristics [3]. Among the diverse realm of MOFs, zirconium-based MOFs (Zr-MOFs) distinguish themselves, demonstrating superior thermal, mechanical, and chemical stabilities in contrast to MOFs with other metal constituents [4,5]. The rational assembly of predesigned building units with strong links into predefined ordered structures has resulted in the discovery of thousands of new MOFs per year that have been employed in diverse applications such as gas storage and separation, renewable energy, environmental applications, catalysis, sensing, and biomedicine [1,6].

Most MOFs have been synthesized using foundational methods, which include the hydrothermal, solvothermal, microwave irradiation, and mechano-chemical processes [7]. The solvothermal method is one such synthesis approach that utilizes solvents at elevated temperatures and pressures to facilitate the formation of crystalline MOF materials [1]. This technique provides precise control over the morphology, size, and composition of MOFs, leading to improved properties and an expanded array of applications. The advancements made in solvothermal synthesis of MOFs underscore the significance of this method in the progress of MOF research.

The synthesis of MOFs commonly involves the deprotonation of organic acids in the presence of metal cations to form metal-oxygen linkages [2]. The rate of deprotonation plays a crucial role in the crystallization process by promoting the development of strong bonds between the inorganic and organic SBUs. The choice of solvents utilized during the synthesis of MOFs based on metal-carboxyl bonding represents one commonly employed strategy to control the rate of deprotonation [7]. This is evidenced by the use of solvent dimethylformamide (DMF), which releases basic amines upon heating [8]. DMF and similar solvents have been successful in growing MOF single crystals in the millimeter range [9].

Heavy metals, such as arsenic (As), cadmium (Cd), and lead (Pb) mercury (Hg), and chromium (Cr), are pernicious water contaminants that pose grave health risks [10–12]. Originating primarily from industrial activities, arsenic contamination in water sources has emerged as a significant threat to both human health and the broader ecosystem. Approximately 140 million individuals across 70 nations ingest water polluted with arsenic that exceed the provisional benchmarks set by the World Health Organization (WHO) [13]. According to the WHO guidelines for drinking-water quality, the maximum acceptable concentration of arsenic in drinking water is set at 10 parts per billion (ppb) [14,15]. Arsenic poisoning has been linked to several human health issues, including diabetes, bronchitis, cardiovascular disease, peripheral neuropathies, and negative reproductive and hematological consequences [16].

The ubiquity of heavy metals like arsenic in natural water sources underscores the pressing need for effective remediation techniques [17–20]. Current remediation paradigms encompass a spectrum of chemical, physical, and biological strategies that have been adopted worldwide. For example, India utilizes reverse osmosis in rural areas while the U.S. favors ion exchange methods [21]. Sustainable and eco-centric biological methods such as bioremediation and biodegradation are garnering interest [22,23]. However, due to its simplicity, cost-effectiveness, and reusability of adsorbents [24–26], the physicochemical approaches using adsorption remain the preferred choice for the elimination of detrimental aquatic contaminants [27–29]. With materials like activated carbon achieving arsenic removal rates of up to 99 %, adsorption has proven particularly effective [30]; however, the choice of sorbent remains a crucial step in determining the process's efficiency [31]. Functionalized MOFs offer promising potential for heavy metal removal in water treatments due to their unique design, high surface area, adjustable pores, and customizable functionalities and dopants [32–44].

Recent attention has been drawn to rare earth elements, especially lanthanum (La), for its distinctive properties and affinity for arsenic (V) [45]. Liu et al. enhanced arsenic removal by combining lanthanum hydroxide and ferric hydroxide with activated carbon, achieving an adsorption rate of 29.44 mg g$^{-1}$ [46]. Similarly, Huang et al. used lanthanum hydroxide-modified vermiculite for phosphate adsorption [47]. These studies underscore the potential of lanthanum in water treatment, particularly when doped into MOFs like MOF-808, optimizing arsenic adsorption by increasing available active sites. The trivalent form, Arsenic (III), is notably carcinogenic and toxic, necessitating its removal from wastewater for health and environmental safety [48].

In this study, La@MOF-808 and MOF-808 were synthesized using the solvothermal technique. The resulting La@MOF-808 and MOF-808 were characterized using a diverse array of analytical techniques such as scanning electron microscopy (SEM), attenuated total reflectance - Fourier transform infrared spectroscopy (ATR-FTIR), X-ray diffraction (XRD), and thermogravimetric analysis (TGA). The MOFs were subsequently employed to measure their effectiveness, stability, and ability to be reused in the process of adsorbing arsenic ions. This study serves as an important initial step in highlighting the potential of La@MOF-808 for remediation of arsenic contamination and emphasizes the need for further research to refine this promising avenue. Notably, this is the first study to investigate the use of La@MOF-808 for the simultaneous removal of both Total As and As(III), an area that has been relatively

unexplored in previous MOF-based studies on arsenic adsorption.

## 2. Experimental section

### 2.1. Material and methods

The chemicals used to synthesize MOF-808 are zirconium oxychloride (98 %), trimesic acid (95 %), formic acid (M: 46.03 g/mol), N, N-Dimethylformamide (99 %), lanthanum trioxide powder (99.9 %), and acetone (M.W: 58.08 g/mol). The chemical used during adsorption studies are sodium hydrogen arsenate ($Na_2HAsO_4 \cdot 7H_2O$, >98 %) and sodium (meta) arsenite ($NaAsO_2$, >90 %), hydrochloric acid (HCl), and sodium hydroxide (NaOH). All chemicals were purchased through Millipore Sigma (Burlington, MA) and used without further purification.

### 2.2. Synthesis of adsorbent material

Zirconium oxychloride (1.82 g) and Trimesic acid (1.12 g) were dissolved in N, N-Dimethylformamide-DMF (50 mL) and formic acid (50 mL) at room temperature. Lanthanum trioxide (1.25 g) was added to the sample and the solution was placed into 200 mL boiling glass beakers. The sample was stirred for an hour at 100 °C and then sonicated for 10 min at a temperature of 40 °C. The same procedure, without the lanthanum addition, was used to create the pristine MOF-808 sample. The samples were covered with aluminum foil and baked for one day at 120 °C. The samples are allowed to cool to room temperature before being filtered with standard filter paper. The filter papers were then warmed in the oven for 12 h at 90 °C to convert the MOFs into powder and are ready for further testing.

### 2.3. Characterizations

Various techniques such as ATR-FTIR, TGA, XRD, and SEM were employed to investigate the synthesized material. The ATR-FTIR spectra was obtained using a Spectrum II instrument (PerkinElmer, Waltham, MA) at a resolution of 400–4000 $cm^{-1}$. A TGA-Q5000 (TA Instruments, New Castle, DE) was utilized to conduct TGA on the samples using the settings: Temperature range: 1000 °C, Mass sensitivity: 0.1 μg, Accuracy: 0.1 % or 10 μg, sample size: 10 mg $g^{-1}$, Heating rate: 10 °C/min, and Temperature range: 100–600 °C. The XRD crystallographic spectra were obtained using a MiniFlex (Rigaku Americas Corporation, The Wooklands, TX) equipped with a copper source (λ = 1.54 Å), and the data were collected in the 2θ range of 10° to 80°. The morphology of the La@MOF-808 was examined using an Apreo Scanning Electron Microscope (ThermoFisher, Pittsburgh, PA) with 0.8 nm resolution achievable at 15 kV and 1.0 nm achievable at 1 kV using the immersion lens. Additionally, the Apreo-SEM is equipped with EDS, EDAX, and EBSD detectors, enhancing its analytical capabilities for elemental analysis and crystallography. An ICP-OES (Agilent 5100) was used to quantify Total As and As(III) concentrations.

### 2.4. Total As and As(III) adsorption experiments

Total As and As(III) removal efficiencies were evaluated with respect to pH (2-10), arsenic concentrations (50–300 ppm), contact duration (5–300 min), and temperature (25–45 °C). It is important to note that, except for the investigation of temperature impact, all the total As and As(III) adsorption tests were conducted at room temperature. Stock solutions were created by dissolving 1 g each of $NaAsO_2$ and $As_2O_3$ in deionized water. Additional concentrations, ranging from 5 to 300 ppm, were achieved by diluting this stock solution. 17.5 mg of the adsorbent material was added to a 50 mL stock solution of Total As and As(III) and shaken at room temperature at 250 rpm for 24 h by following a previously reported procedure. Samples were filtered using a 0.2 μm filter and the concentrations of Total As and As(III) were measured using the ICP-OES.

Eq. (1) [49] was used to compute the equilibrium adsorption capacity of Total As and As(III):

$$q_e = \frac{(C_O - C_e)\,V}{m} \tag{1}$$

The mass of target pollutants adsorbed at equilibrium ($q_e$) was expressed in mg $g^{-1}$. The initial pollutant concentration ($C_o$) and the equilibrium pollutant concentration ($C_e$) were both expressed in mg/liter. The volume of solution for Total As and As(III) was in milliliters, while the quantity of adsorbent (m) was in milligrams. Adsorption trials were carried out three times for each sample, with the average results utilized to determine the adsorption amount. To investigate the optimum adsorption time, a kinetic study was carried out. Individual tubes were extracted from the shaker at intervals of 5, 50, 100, 150, 200, 250–300 min. To examine the impact of pH, solutions were adjusted using 1.0 M HCl and 2.0 M NaOH solutions in single increments from 2 to 10. The effect of temperature [50], was evaluated by varying temperatures from 25 to 45 °C with 10 °C increments.

## 3. Results and discussion

### 3.1. Synthesis effectiveness

La@MOF-808 was synthesized using solvothermal synthesis. Solvothermal synthesis provides better control over the reaction

conditions and produces high-quality crystals but is more time-consuming. Given the higher quality product created by the solvothermal method we elected to use those samples for the arsenic removal studies.

### 3.2. Characterizations

The SEM analysis of both samples revealed distinct differences in their morphology at different magnifications Fig. 1. At 2 μm, the MOF-808 Fig. 1(a) sample exhibited cracks and voids, while the La@MOF-808 Fig. 1(b) sample displayed rod-like shape well defined crystals. These observations are consistent with previous research, where the introduction of lanthanum slightly damaged the MOF-808 structure, resulting in smaller particle sizes compared to the lanthanum-free material. Overall, these findings indicate the influence of lanthanum doping on the morphology and particle size distribution of MOF-808, highlighting potential implications for its properties. EDX mapping analysis of La@MOF-808 sample (Fig. S1) revealed the presence of oxygen, zirconium and lanthanum which was observed 36.34 %, 3.57 % and 1.28 %, respectively. This indicates that these elements were uniformly distributed within the nanopolyhedral framework. This even distribution of elements helps prevent agglomeration, which is often observed after metal modification [49,51]. Furthermore, the EDX mapping analysis revealed a high degree of overlapping distribution between lanthanum and oxygen elements, indicating a strong correlation between these two. This observation, suggests that lanthanum reacted with the ligands in the MOF-808 framework, acting as metal centers to form La-BTC. These findings demonstrate the successful incorporation of lanthanum into the MOF-808 structure, providing valuable insights into the composition and potential properties of the La@MOF-808 sample.

The surface functional groups of the designed adsorbents are identified using ATR-FTIR spectroscopy within a scanning range of 500–3500 $cm^{-1}$. The plot clearly shows distinct peaks corresponding to different functional groups in each sample. Fig. 2(a) displays the spectra of both MOF-808 (red line) and La@MOF-808 (black line), illustrating the differences in their functional group compositions. For the MOF-808 sample, the following functional groups were identified at specific wavenumbers: C–H bonds at 2912 $cm^{-1}$, C=O at 1716 $cm^{-1}$, N–H at 1572 $cm^{-1}$, carboxylic acids at 1423 $cm^{-1}$, and alkyl halides and amines in the range of 777–1188 $cm^{-1}$ with small sharp peaks. Additionally, there were peaks observed in the range of 449–651 $cm^{-1}$. Similarly, the FTIR spectra of the La@MOF-808 sample exhibited peaks corresponding to various functional groups. These included C–H bonds at 2927 $cm^{-1}$, C=O at 1715, N–H at 1571 $cm^{-1}$, carboxylic acids at 1423 $cm^{-1}$, and alkyl halides and amines in the range of 776–1178 $cm^{-1}$ with small sharp peaks. Additionally, there were peaks observed in the range of 451–758 $cm^{-1}$. The shift in the positions of these functional group peaks following the doping of MOF-808 with lanthanum metal indicates the disruption or modification of loaded molecules [51]. Notably, characteristic peaks related to O–C–O symmetric and asymmetric stretching vibrations were observed at 1667-1571 $cm^{-1}$ and 1428-1354 $cm^{-1}$, respectively. This confirms the interaction between metal ions and carboxylic acids present in the MOF-808 structure. Furthermore, an additional observation can be made from the spectra. In the MOF-808 spectrum, there is a characteristic peak near 754 $cm^{-1}$, which corresponds to the stretching vibration of Zr–O bonds. However, in the spectrum of La@MOF-808, a modest new peak appears at 501 $cm^{-1}$, indicating the stretching vibration of La–O bonds. This suggests that the introduction of lanthanum resulted in the formation of La–O–Zr bonds through a condensation reaction [51]. Therefore, it can be concluded that lanthanum has been successfully loaded onto the MOF-808 material.

XRD patterns for both MOF-808 (red line) and La@MOF-808 (black line) are presented in Fig. 2(b). The diffraction peaks observed in the XRD pattern of MOF-808 aligned perfectly with those of the standard MOF-808 crystal. This correspondence in diffraction peaks
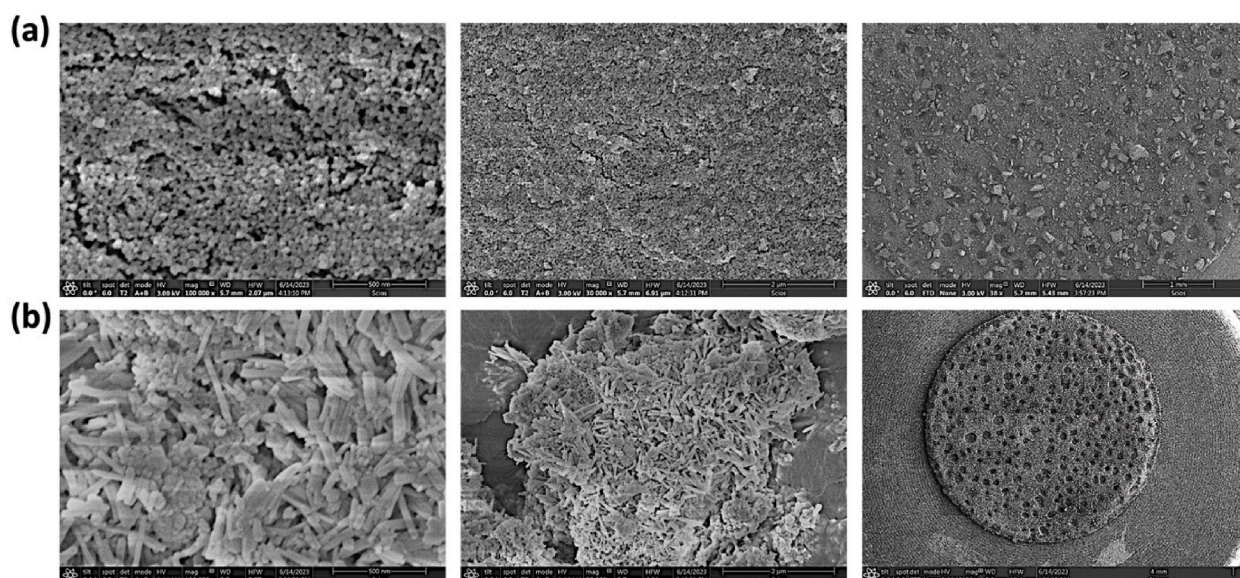


**Fig. 1.** Scanning electron micrographs of (a) MOF-808 and (b) La@MOF-808 samples.
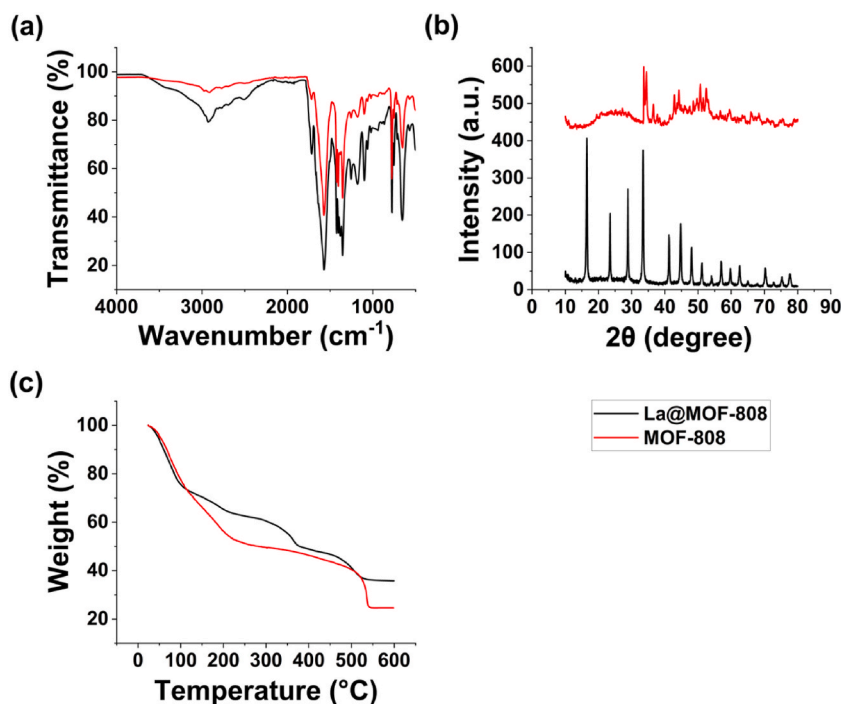
**Fig. 2.** (a) ATR-FTIR, (b) XRD, and (c) TGA spectra for MOF-808 (red) and La@MOF-808 (black) samples. (For interpretation of the references to colour in this figure legend, the reader is referred to the Web version of this article.)

confirms the high purity of the MOF-808 sample, indicating that it is composed of the expected crystalline structure without any significant impurities or deviations. The excellent crystallization of La@MOF-808 sample is clearly demonstrated by the distinct peaks observed in that figure. La@MOF-808 sample exhibited distinctive peaks at $2\theta = 16.49°$, $23.51°$, $28.86°$, and $33.33°$ at intensity (a.u.) 425.11, 209.72, 274.49, and 383.56, respectively. In La@MOF-808 sample, the peaks are significantly intensified compared to MOF-808 sample, which indicates that the crystallinity of MOF-808 remains unaffected after the introduction of lanthanum oxide and its structural framework remains intact without the introduction oxide impurities. Furthermore, in the La@MOF-808 samples, certain peaks, such as those at 16°, 17°, 23°, 29°, 41.2°, 44.8°, and 48.02° exhibit notable enhancements [49,51]. This provides further confirmation that the lanthanum nanoparticles are effectively dispersed throughout the MOF-808 structure upon incorporation. The emergence of these new peaks suggests the presence of new crystalline phases or compounds. Some peaks almost disappeared in pristine MOF-808, which may be due to the reduction in the number of Zr–O clusters, which was not conducive to the adsorption of arsenic ions [51]. The introduction of these nanoparticles in MOF-808 resulted in a significant increase in the degree of crystallinity. This enhancement in crystallinity suggests that the incorporation of lanthanum in the MOF-808 framework has played a role in the formation of a well-organized structure within the backbone chains. This well-organized structure is believed to be responsible for the observed increase in crystallinity, as suggested by previous studies. Hence, meticulous control of the lanthanum material is necessary to prevent excessive damage to the crystal structure of MOF-808 and preserve its adsorption capacity.

The TGA results, which are depicted in Fig. 2(c), demonstrated distinct differences in the thermal behavior and weight loss profiles of MOF-808 (red line) and La@MOF-808 (back line). During the study, MOF-808 underwent two weight loss events at 0–251 °C (51.1 %) and 252–538 °C (26 %). In contrast, La@MOF-808 exhibited three different weight loss events at 0–137 °C (29.7 %), 138–367 °C (20 %), and 368–541 °C (17 %). These weight loss events indicate that the material undergoes multiple decomposition reactions at different temperatures [49]. The first weight loss event is likely due to the evaporation of any residual solvents or water molecules adsorbed onto the surface of the material. The subsequent weight loss events at higher temperatures suggest the decomposition of the MOF-808 framework and/or the organic ligands and the release of volatile products. The presence of lanthanum metal in the material may contribute to stability of the material and minimize some of the weight loss events, as it may undergo thermal decomposition at certain temperatures. This was achieved by determining the number of absent linkers in both samples, following a previously published method [52]. The underlying principle of this approach is based on the inverse relationship between the weight loss plateau, which is associated with linker combustion, and the number of absent linkers present in the structure [52]. By applying this comparison, the data suggests that MOF-808 has a higher number of linkers and therefore illustrates a higher weight loss upon their combustion.

### 3.3. Adsorption study

Following peer-reviewed literature [50], adsorption capacity experiments for Total As and As(III) was conducted on both samples

with replicates at varying concentrations ranging from 50 to 300 ppm Fig. 3. When testing As(III) at a concentration of 100 ppm, the La@MOF-808 samples demonstrated promising outcomes of 98.7 % removal efficiency. On the other hand, when Total As was tested at the same concentration, the outcome for this sample was 98.2 %. However, the MOF-808 sample yielded a less favorable result of Total As and As(III), comparatively, in as showed in Fig. 3. Based on the results depicted in Fig. 3, it can be observed that the removal efficiency rose as the concentration of the solute increased. However, the adsorption capacity reached a plateau or saturation point at 250 ppm. On the other hand, the adsorption rate was found to be highest at a concentration of 100 ppm. The La@MOF-808 had a promising adsorption performance at different concentrations as compared to other samples. This trend can be attributed to the higher concentration gradient, which provides a larger mass transfer and more available active sites on the MOF surface, thereby increasing the probability of surface adsorption.

The saturated adsorption capacity for Total As and As(III) reached 282.9 mg g$^{-1}$ and 283.5 mg g$^{-1}$, respectively, for La@MOF-808 versus 229.7 mg g$^{-1}$ and 239.1 mg g$^{-1}$, respectively, for to MOF-808 (Fig. S2). The enhanced adsorption capacity observed for La@MOF-808 can be attributed to the impact of lanthanum doping, which yielded larger pore diameter for La@MOF-808 in comparison to MOF-808. These results clearly demonstrate the significant impact of lanthanum modification on the adsorption performance.

The aforementioned data were analyzed using Langmuir Eq. (2) and Freundlich models Eq. (3) [50].

$$q_e = \frac{q_m K_L C_e}{1} + K_L C_e \qquad (2)$$

$$\text{Log } q_e = \text{Log } K_F + \frac{1}{n} \text{Log } C_e \qquad (3)$$

in Table 1 the Langmuir model predicted maximum adsorption capacities ($q_{max}$) of La@MOF-808 was 307.7 mg g$^{-1}$ for Total As and 325.7 mg g$^{-1}$ for As(III), surpassing those of MOF-808 adsorbent (Fig. S3). The enhanced adsorption performance can be attributed to the high specific surface area and the abundance of active sites on the adsorbent material. The results indicated that the Langmuir model (Fig. S3) is more suitable for La@MOF-808 than the Freundlich model (Fig. S4) for describing the adsorption of Total As and As (III) on both materials. This is due to the higher correlation coefficient $R^2$ achieved by the Langmuir model, indicating that these processes involve monolayer adsorption [51].

### 3.4. Influence of pH

Due to changes in the adsorbent's structure and surface charge as well as the speciation of Total As/As(III) ions, the adsorption process is significantly influenced by pH. For example, pH has a direct influence on the behavior of arsenic species in solution [50]. At a pH lower than 2.1, arsenic exists as arsenic acid ($H_3AsO_4$). As the pH increases from 2.1 to 6.7, the dominant arsenic species transition from the monohydrogen arsenate ion ($H_2AsO_4^-$) to the dihydrogen arsenate ion ($HAsO_4^{2-}$). These transformations occur through protonation and deprotonation processes as arsenic acid interacts with water, and the relative abundance of these forms change with pH.

To characterize the impact of pH on the ability of MOF-808 and La@MOF-808 to adsorb Total As/As(III) ions, numerous batch experiments were undertaken. These experiments were designed to quantify the removal rate of Total As and As(III) over the pH range of 2.0–10.0. All experiments were conducted under ambient conditions (temperature maintained at $25 \pm 1$ °C) using an adsorbent dose
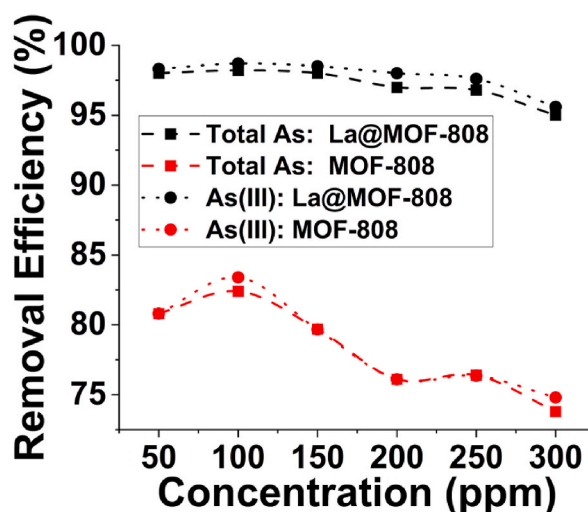


**Fig. 3.** Assessment of Total As (square) and As(III) (circle) removal efficiency for La@MOF-808 (black) and MOF-808 (red) samples. (For interpretation of the references to colour in this figure legend, the reader is referred to the Web version of this article.)

**Table 1**

Isotherm Model Parameters for the Removal of Total As and As(III) using MOF-808 and La@MOF-808

| Material | Pollutant | Langmuir Model | | | Freundlich Model | | |
|---|---|---|---|---|---|---|---|
| | | $q_m$ (mg g$^{-1}$) | $K_L$ (L mg$^{-1}$) | $R^2$ | $K_F$ | $\frac{1}{n}$ | $R^2$ |
| **MOF-808** | Total As | 133.7 | 0.225 | 0.8484 | 8.93 | 0.51038 | 0.7525 |
| | As(III) | 161.8 | 0.0186 | 0.8766 | 8.24 | 0.55596 | 0.8021 |
| **La@MOF-808** | Total As | 307.7 | 0.189 | 0.9918 | 62.53 | 0.44944 | 0.8226 |
| | As(III) | 325.7 | 0.181 | 0.9911 | 63.40 | 0.46266 | 0.8267 |

of 17.5 mg, a contact time of 180 min, and an initial concentration of 100 ppm for both Total As and As(III).

The removal efficiency of Total As (square) and As(III) (circle) for MOF-808 (red) and La@MOF-808 (black) as a function of pH are illustrated in Figure (4). The highest percentage of both pollutants Total As and As(III) removal was achieved at pH 5.0 Figure (4). For Total As, the removal rates were 98.8 %, and 84.6 % for both samples at pH 5.0. On the other hand, for As(III) at the same pH, the removal rates were 98.8 %, and 85.6 %, respectively. The reduction in arsenic removal at higher pH levels could be due to two reasons. Firstly, when the concentration of H$^+$ ions in the water is high, the positive charge over the amino group increases. Secondly, excessive amounts of hydroxyl ions present in the water at alkaline pH levels can compete for active sites [53]. At low pH levels, the adsorbent's surface possessed a greater positive charge, which facilitated adsorption process [51,54]. The observation of the highest adsorption capacity near a pH of 7.0 suggests that the adsorption of Total As and As(III) on the adsorbent is not solely driven by electrostatic attraction but also involves chemical complexation. This indicates that there are additional interactions occurring between the adsorbent and the arsenic species beyond simple electrostatic forces. However, the low adsorption capacity observed at highly alkaline (pH 10.0) pH levels was attributed to the dissolution of La@MOF-808, as depicted in Fig. 4. In comparison with Total As, the As(III) adsorption rate of all the samples are more efficient at different pH conditions. Therefore, maintaining the pH within the range of 2.0–7.0 ensures optimal conditions for effective adsorption onto the adsorbent.

### 3.5. Kinetic study

To investigate the mechanism behind Total As and As(III) adsorption, it is essential to gain a practical understanding of the kinetics of Total As and As(III) adsorption on La@MOF-808 and MOF-808 samples. To examine the adsorption rate, the Total As and As(III) uptake was studied as a function of contact time, and the results were presented in Table 2. It was observed that the remaining Total As and As(III) concentration declined with time gradients until equilibrium was reached. The La@MOF-808 sample exhibited higher and faster adsorption as compared to MOF-808, likely due to the availability of more adsorption sites in structure. For further exploration, two kinetic models, namely pseudo-first-order Eq. (4) [50] and pseudo-second-order models Eq. (5) [55], were used to extract the kinetic parameters of the adsorption process.

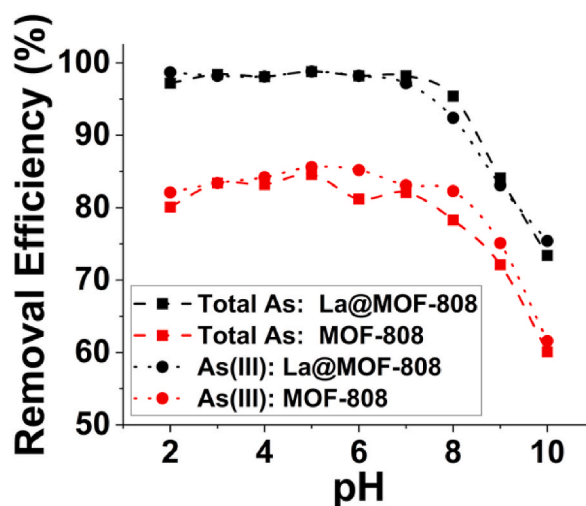$$\ln(q_e - q_t) = \ln(q_e) - k_1 t \qquad (4)$$



**Fig. 4.** The impact of pH on the removal efficiency of Total As (square) and As(III) (circle) for La@MOF-808 (black) and MOF-808 (red) samples. (For interpretation of the references to colour in this figure legend, the reader is referred to the Web version of this article.)

**Table 2**

Kinetic Model Parameters for the Removal of Total As and As(III) using MOF-808 and La@MOF-808

| Material | Pollutant | Pseudo First Order | | | Pseudo Second Order | |
|---|---|---|---|---|---|---|
| | | $q_{(cal)}$ (mg/g) | $k_1$ (min) | $R^2$ | $q_{(cal)}$ (mg/g) | $R^2$ |
| MOF-808 | Total As | 131.42 | 1.09 | 0.992 | 162.34 | 0.930 |
| | As(III) | 156.33 | 7.77 | 0.988 | 169.78 | 0.931 |
| La@MOF-808 | Total As | 285.73 | 9.03 | 0.976 | 330.03 | 0.989 |
| | As(III) | 301.84 | 8.11 | 0.974 | 335.57 | 0.991 |

$$\frac{t}{q_t} = \frac{1}{k_2 q_e^2} + \frac{t}{q_t} \tag{5}$$

The experimental determination of the equilibrium adsorption capacity is represented by $q_e$ (mg g$^{-1}$), while the adsorption quantity at time t is represented by $q_t$ (mg g$^{-1}$). The pseudo-first-order rate constant is represented by $k_1$ (min$^{-1}$), while the pseudo-second-order rate constant is represented by $k_2$ (g mg$^{-1}$ min$^{-1}$). In case of La@MOF-808 sample, the correlation coefficients ($R^2$) obtained from the pseudo-second-order model were found to be greater than those obtained from the pseudo-first-order model (Fig. S5). Based on these findings, it can be concluded that the adsorption kinetics of La@MOF-808 followed the pseudo-second-order model (Fig. S6). This suggests that the chemisorption process is strong, and the surface is capable of greatly adsorbing Total As and As (III) [51].

### 3.6. Thermodynamic study

The impact of temperature on the adsorption process was investigated by studying the uptake of Total As and As(III) by an adsorbent material at temperatures ranging from 25 °C to 45 °C. Additionally, various thermodynamic parameters, such as ΔG (T), ΔS (T), and ΔH (T), were calculated eqs. (6)–(8) [56,57].

$$\Delta G° = - RT \ln K_c \tag{6}$$

$$\text{Log } K_c = \frac{\Delta S (T)}{R} - \frac{\Delta H (T)}{RT} \tag{7}$$

$$\Delta G (T) = \Delta H(T) - T\Delta S (T) \tag{8}$$

These parameters were calculated using the ideal gas constant (R = 8.314 J mol$_{-1}$ K$^{-1}$), the thermodynamic equilibrium constant of adsorption ($K_c$), and the absolute temperature (T). The experimental data was plotted, and it was observed that there exists a linear relationship between the natural logarithm of Kc (lnK) and the reciprocal of the temperature (1/T). By analyzing this relationship, the corresponding thermodynamic parameters were determined and summarized in Table 2. Remarkably, the experimental outcomes demonstrated that the ΔG° values for the adsorption of Total As and As(III) onto the surface of La@MOF-808 were consistently
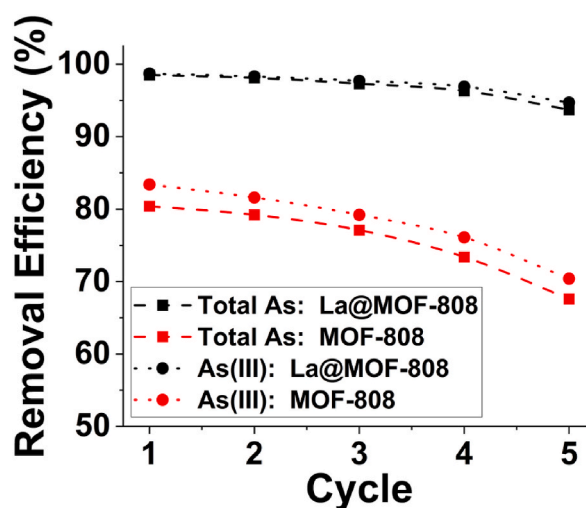


**Fig. 5.** Reusability test results depicting removal efficiency of Total As (square) and As(III) (circle) for La@MOF-808 (black) and MOF-808 (red) samples over the course of five cycles. (For interpretation of the references to colour in this figure legend, the reader is referred to the Web version of this article.)

negative across all temperature variations. This compelling evidence confirms that both adsorption processes were spontaneous in nature [51]. On the other hand, the ΔH° values, indicative of the standard enthalpy change, were found to be positive. This positive ΔH° signifies that the adsorption reactions involving these two species were endothermic processes, requiring an input of energy. It can be inferred that higher temperatures enhanced the adsorbent's ability to effectively capture the target anions. Another important aspect of the thermodynamic analysis was the evaluation of the standard entropy change (ΔS°) during the adsorption process. Notably, all ΔS° values were found to be positive, indicating an increase in disorder at the solid-liquid interface. This rise in entropy suggests that the adsorption of Total As and As(III) onto the La@MOF-808 led to greater molecular randomness and an increased degree of freedom. These findings align with previous conclusions [54].

### 3.7. Reusability test

Overall, the reusability experiment showed that La@MOF-808 has good stability and reproducibility as an adsorbent for Total As and As(III) removal. Fig. 5 depicts a consistently high removal rate of La@MOF-808, even after five cycles, in contrast to MOF-808. Moreover, the material maintained its original structure. La@MOF-808 after five cycles, likely due to the precise La@MOF-808 concentration ratio used in developing this innovative material. This suggests that La@MOF-808 sample exhibits promising application prospects for the removal of Total As or As(III) from water samples. For As(III), the removal rate of La@MOF-808 is excellent as compared to Total As from Total As/As(III) contaminated water samples. This is consistent with previous studies that have shown that MOFs preferentially adsorb As(III) [49–51,54]. This study's significance lies in its ability to predict the practical applications of La@MOF-808 in removing Total As and As(III) from polluted water sources.

## 4. Conclusion

In the presented study, La@MOF-808 has been identified as a proficient adsorbent for the remediation of Total As and As(III) from water. Utilizing the solvothermal method, the La@MOF-808 was synthesized, exhibiting a porous nature and a superior specific surface area. Structural characterization via ATR-FTIR and XRD analyses further confirmed its distinct functional group variations when juxtaposed against standard MOF-808. Furthermore, our findings reveal that La@MOF-808 demonstrated an impressive maximum adsorption capacity, achieving 307.7 mg g$^{-1}$ for Total As and 325.7 mg g$^{-1}$ for As(III). This proficiency not only outperforms many existing adsorbents but also aligns with the Langmuir model thereby suggesting monolayer adsorption. The material's efficacy is most notable within a pH range of 2.0–7.0, emphasizing its selectivity. Thermodynamic assessments posit that the adsorption process on La@MOF-808 is spontaneous and endothermic in nature. After enduring multiple sorption-desorption cycles, the stability and efficiency of La@MOF-808 remain commendable. The primary adsorption mechanisms, as indicated by our analyses, seem to involve ligand exchange and electrostatic attractions.

In conclusion, La@MOF-808 stands out as a promising solution for arsenic ion removal. Lanthanum doping markedly enhances MOF-808's arsenic removal, underscoring its potential for water treatment. The union of ligand exchange and electrostatic attractions not only ensures the efficient capture of arsenic contaminants but also signals La@MOF-808's adaptability to capture other potential pollutants. Such versatility mandates further exploration into its broader applications, extending beyond arsenic sequestration. The structure of La@MOF-808, while exhibiting significant arsenic removal capabilities, presents a favorable environmental profile; however, it is imperative to consider the long-term environmental ramifications. The introduction of lanthanum, though enhancing adsorptive capabilities, could pose ecological risks if released into water ecosystems in significant quantities. Lanthanum's potential bioaccumulation might disrupt aquatic life, impacting the food chain.

As La@MOF-808 shines in a controlled setting, its true potential will be unveiled through real-world application tests in diverse wastewater environments. Successful adaptation in such scenarios could catalyze the development of globally scalable, sustainable water treatment solutions, directly addressing the pressing issue of arsenic contamination and potentially other waterborne pollutants.

### CRediT authorship contribution statement

**Hassan Nawaz:** Conceptualization, Data curation, Formal analysis, Writing – original draft, Writing – review & editing. **Muhammad Ibrahim:** Conceptualization, Funding acquisition, Methodology, Project administration, Supervision. **Abid Mahmood:** Conceptualization, Supervision. **Gregg P. Kotchey:** Formal analysis, Investigation, Methodology, Validation, Visualization, Writing – review & editing. **David V.P. Sanchez:** Data curation, Formal analysis, Funding acquisition, Methodology, Project administration, Resources, Supervision, Visualization, Writing – review & editing.

### Declaration of competing interest

The authors declare that they have no known competing financial interests or personal relationships that could have appeared to influence the work reported in this paper.

### Appendix A. Supplementary data

Supplementary data to this article can be found online at https://doi.org/10.1016/j.heliyon.2023.e21572.

# References

[1] H. Furukawa, K.E. Cordova, M. O'Keeffe, O.M. Yaghi, The chemistry and applications of metal-organic frameworks, Science 341 (2013), 1230444, https://doi.org/10.1126/science.1230444.

[2] J. Jiang, Y. Zhao, O.M. Yaghi, Covalent chemistry beyond molecules, J. Am. Chem. Soc. 138 (2016) 3255–3265, https://doi.org/10.1021/jacs.5b10666.

[3] O.M. Yaghi, M. O'Keeffe, N.W. Ockwig, H.K. Chae, M. Eddaoudi, J. Kim, Reticular synthesis and the design of new materials, Nature 423 (2003) 705–714, https://doi.org/10.1038/nature01650.

[4] H. Wu, T. Yildirim, W. Zhou, Exceptional mechanical stability of highly porous zirconium metal–organic framework uio-66 and its important implications, J. Phys. Chem. Lett. 4 (2013) 925–930, https://doi.org/10.1021/jz4002345.

[5] J.H. Cavka, S. Jakobsen, U. Olsbye, N. Guillou, C. Lamberti, S. Bordiga, K.P. Lillerud, A new zirconium inorganic building brick forming metal organic frameworks with exceptional stability, J. Am. Chem. Soc. 130 (2008) 13850–13851, https://doi.org/10.1021/ja8057953.

[6] M. Kurmoo, Magnetic metal–organic frameworks, Chem. Soc. Rev. 38 (2009) 1353, https://doi.org/10.1039/b804757j.

[7] N. Stock, S. Biswas, Synthesis of metal-organic frameworks (mofs): routes to various mof topologies, morphologies, and composites, Chem. Rev. 112 (2012) 933–969, https://doi.org/10.1021/cr200304e.

[8] H. Li, M. Eddaoudi, T.L. Groy, O.M. Yaghi, Establishing microporosity in open metal−organic frameworks: gas sorption isotherms for zn(bdc) (bdc = 1,4-benzenedicarboxylate), J. Am. Chem. Soc. 120 (1998) 8571–8572, https://doi.org/10.1021/ja981669x.

[9] L. Li, F. Sun, J. Jia, T. Borjigin, G. Zhu, Growth of large single mof crystals and effective separation of organic dyes, CrystEngComm 15 (2013) 4094, https://doi.org/10.1039/c3ce40137e.

[10] G. Mladin, M. Ciopec, A. Negrea, N. Duteanu, P. Negrea, P. Ianasi, C. Ianasi, Silica- iron oxide nanocomposite enhanced with porogen agent used for arsenic removal, Materials 15 (2022) 5366, https://doi.org/10.3390/ma15155366.

[11] M. Ciopec, G. Biliuta, A. Negrea, N. Duteanu, S. Coseri, P. Negrea, M. Ghangrekar, Testing of chemically activated cellulose fibers as adsorbents for treatment of arsenic contaminated water, Materials 14 (2021) 3731, https://doi.org/10.3390/ma14133731.

[12] M. Samimi, M. Shahriari-Moghadam, Isolation and identification of delftia lacustris strain-ms3 as a novel and efficient adsorbent for lead biosorption: kinetics and thermodynamic studies, optimization of operating variables, Biochem. Eng. J. 173 (2021), 108091, https://doi.org/10.1016/j.bej.2021.108091.

[13] P. Ravenscroft, H. Brammer, K. Richards, Arsenic in Asia. Arsenic Pollution: A Global Synthesis, Wiley-Blackwell, Chichester, UK, 2009, pp. 318–386.

[14] M. Jian, B. Liu, G. Zhang, R. Liu, X. Zhang, Adsorptive removal of arsenic from aqueous solution by zeolitic imidazolate framework-8 (zif-8) nanoparticles, Colloids Surf Physicochem Eng Aspects 465 (2015) 67–76, https://doi.org/10.1016/j.colsurfa.2014.10.023.

[15] H. Atallah, M Elcheikh Mahmoud, A. Jelle, A. Lough, M. Hmadeh, A highly stable indium based metal organic framework for efficient arsenic removal from water, DTr 47 (2018) 799–806, https://doi.org/10.1039/C7DT03705H.

[16] M. Ciopec, C.M. Davidescu, A. Negrea, N. Duteanu, G. Rusu, O. Grad, P. Negrea, Amberlite xad7 resin functionalized with crown ether and fe(iii) used for arsenic removal from water, Pure Appl. Chem. 91 (2019) 375–388, https://doi.org/10.1515/pac-2018-0607.

[17] S. Zhang, J. Wang, Y. Zhang, J. Ma, L. Huang, S. Yu, et al., Applications of water-stable metal-organic frameworks in the removal of water pollutants: a review, Environ. Pollut. 291 (2021), 118076, https://doi.org/10.1016/j.envpol.2021.118076.

[18] Z. Ullah, A. Rashid, J. Ghani, Talib Ma, A. Shahab, L. Lun, Arsenic contamination, water toxicity, source apportionment, and potential health risk in groundwater of jhelum basin, Punjab, Pakistan, Biol. Trace Elem. Res. 201 (2023) 514–524, https://doi.org/10.1007/s12011-022-03139-0.

[19] Q. Gao, J. Xu, X.-H. Bu, Recent advances about metal–organic frameworks in the removal of pollutants from wastewater, Coord. Chem. Rev. 378 (2019) 17–31, https://doi.org/10.1016/j.ccr.2018.03.015.

[20] B. Aghel, M. Mohadesi, A. Gouran, M.H. Razmegir, Use of modified iranian clinoptilolite zeolite for cadmium and lead removal from oil refinery wastewater, Int. J. Environ. Sci. Technol. 17 (2020) 1239–1250, https://doi.org/10.1007/s13762-019-02466-5.

[21] A.J. Gadgil, S. Amrose, D. Hernandez, Stopping Arsenic Poisoning in india. Introduction to Development Engineering, Springer International Publishing, Cham, 2023, pp. 359–398.

[22] K. Chandra Sekhar, C.T. Kamala, N.S. Chary, Y. Anjaneyulu, Removal of heavy metals using a plant biomass with reference to environmental control, Int. J. Miner. Process. 68 (2003) 37–45, https://doi.org/10.1016/S0301-7516(02)00047-9.

[23] Murugesan Nam, Kim Ryu, Arsenic (as) removal using talaromyces sp. Km-31 isolated from as-contaminated mine soil, Minerals 9 (2019) 568, https://doi.org/10.3390/min9100568.

[24] X. Li, B. Wang, Y. Cao, S. Zhao, H. Wang, X. Feng, et al., Water contaminant elimination based on metal–organic frameworks and perspective on their industrial applications, ACS Sustain. Chem. Eng. 7 (2019) 4548–4563, https://doi.org/10.1021/acssuschemeng.8b05751.

[25] M.K. Uddin, A review on the adsorption of heavy metals by clay minerals, with special focus on the past decade, Chem. Eng. J. 308 (2017) 438–462, https://doi.org/10.1016/j.cej.2016.09.029.

[26] E. Demirbas, Adsorption of cobalt(ii) ions from aqueous solution onto activated carbon prepared from hazelnut shells, Adsorpt. Sci. Technol. 21 (2003) 951–963, https://doi.org/10.1260/02636170360744380.

[27] A. Asghar, M.M. Bello, A.A.A. Raman, Metal-organic frameworks for heavy metal removal, Appl. Water Sci. (2021) 321–356. Wiley.

[28] Z. Rao, K. Feng, B. Tang, P. Wu, Surface decoration of amino-functionalized metal–organic framework/graphene oxide composite onto polydopamine-coated membrane substrate for highly efficient heavy metal removal, ACS Appl. Mater. Interfaces 9 (2017) 2594–2605, https://doi.org/10.1021/acsami.6b15873.

[29] H. Moayedi, B. Aghel, MaM. Abdullahi, H. Nguyen, A.Safuan A. Rashid, Applications of rice husk ash as green and sustainable biomass, J. Clean. Prod. 237 (2019), 117851, https://doi.org/10.1016/j.jclepro.2019.117851.

[30] L. Hao, M. Liu, N. Wang, G. Li, A critical review on arsenic removal from water using iron-based adsorbents, RSC Adv. 8 (2018) 39545–39560, https://doi.org/10.1039/C8RA08512A.

[31] A. Gabor, C.M. Davidescu, A. Negrea, M. Ciopec, L. Lupa, Behaviour of silica and florisil as solid supports in the removal process of as(v) from aqueous solutions, J. Anal. Method. Chem. 2015 (2015) 1–10, https://doi.org/10.1155/2015/562780.

[32] M. Samimi, M. Safari, Tmu-24 (zn-based mof) as an advance and recyclable adsorbent for the efficient removal of eosin b: characterization, equilibrium, and thermodynamic studies, Environ. Prog. Sustain. Energy 41 (2022), e13859, https://doi.org/10.1002/ep.13859.

[33] H. Ehzari, M. Safari, M. Samimi, Signal amplification of novel sandwich-type genosensor via catalytic redox-recycling on platform mwcnts/fe3o4@tmu-21 for brca1 gene detection, Talanta 234 (2021), 122698, https://doi.org/10.1016/j.talanta.2021.122698.

[34] H.-C. Zhou JR Long, O.M. Yaghi, Introduction to metal–organic frameworks, Chem. Rev. 112 (2012) 673–674, https://doi.org/10.1021/cr300014x.

[35] D. Farrusseng, S. Aguado, C. Pinel, Metal-organic frameworks: opportunities for catalysis, Angew. Chem. Int. Ed. 48 (2009) 7502–7513, https://doi.org/10.1002/anie.200806063.

[36] J.-R. Li, R.J. Kuppler, H.-C. Zhou, Selective gas adsorption and separation in metal–organic frameworks, Chem. Soc. Rev. 38 (2009) 1477, https://doi.org/10.1039/b802426j.

[37] Y. Cui, B. Li, H. He, W. Zhou, B. Chen, G. Qian, Metal–organic frameworks as platforms for functional materials, Acc. Chem. Res. 49 (2016) 483–493, https://doi.org/10.1021/acs.accounts.5b00530.

[38] J.-R. Li, J. Sculley, H.-C. Zhou, Metal–organic frameworks for separations, Chem. Rev. 112 (2012) 869–932, https://doi.org/10.1021/cr200190s.

[39] G. Lin, B. Zeng, J. Li, Z. Wang, S. Wang, T. Hu, L. Zhang, A systematic review of metal organic frameworks materials for heavy metal removal: synthesis, applications and mechanism, Chem. Eng. J. 460 (2023), 141710, https://doi.org/10.1016/j.cej.2023.141710.

[40] M. Jian, B. Liu, R. Liu, J. Qu, H. Wang, X. Zhang, Water-based synthesis of zeolitic imidazolate framework-8 with high morphology level at room temperature, RSC Adv. 5 (2015) 48433–48441, https://doi.org/10.1039/C5RA04033G.

[41] P. Falcaro, R. Ricco, C.M. Doherty, K. Liang, A.J. Hill, M.J. Styles, Mof positioning technology and device fabrication, Chem. Soc. Rev. 43 (2014) 5513–5560, https://doi.org/10.1039/C4CS00089G.

[42] M. Shahsavari, P. Mohammadzadeh Jahani, I. Sheikhshoaie, S. Tajik, A Aghaei Afshar, M.B. Askari, et al., Green synthesis of zeolitic imidazolate frameworks: a review of their characterization and industrial and medical applications, Materials 15 (2022) 447, https://doi.org/10.3390/ma15020447.

[43] B. Shen, B. Wang, L. Zhu, L. Jiang, Properties of cobalt- and nickel-doped zif-8 framework materials and their application in heavy-metal removal from wastewater, Nanomaterials 10 (2020) 1636, https://doi.org/10.3390/nano10091636.

[44] H. Ehzari, M. Amiri, M. Safari, M. Samimi, Zn-based metal-organic frameworks and p-aminobenzoic acid for electrochemical sensing of copper ions in milk and milk powder samples, Int. J. Environ. Anal. Chem. 102 (2022) 4364–4377, https://doi.org/10.1080/03067319.2020.1784410.

[45] R.S.S. Wu, K.H. Lam, J.M.N. Lee, T.C. Lau, Removal of phosphate from water by a highly selective la(iii)-chelex resin, Chemosphere 69 (2007) 289–294, https://doi.org/10.1016/j.chemosphere.2007.04.022.

[46] J. Liu, Q. Zhou, J. Chen, L. Zhang, N. Chang, Phosphate adsorption on hydroxyl–iron–lanthanum doped activated carbon fiber, Chem. Eng. J. 215–216 (2013) 859–867, https://doi.org/10.1016/j.cej.2012.11.067.

[47] W.-Y. Huang, D. Li, Z.-Q. Liu, Q. Tao, Y. Zhu, J. Yang, Y.-M. Zhang, Kinetics, isotherm, thermodynamic, and adsorption mechanism studies of la(oh) 3 -modified exfoliated vermiculites as highly efficient phosphate adsorbents, Chem. Eng. J. 236 (2014) 191–201, https://doi.org/10.1016/j.cej.2013.09.077.

[48] World Health O, Global Reference List of 100 Core Health Indicators (Plus Health-Related Sdgs), World Health Organization, Geneva, 2018, 2018.

[49] N. Assaad, G. Sabeh, M. Hmadeh, Defect control in zr-based metal–organic framework nanoparticles for arsenic removal from water, ACS Appl. Nano Mater. 3 (2020) 8997–9008, https://doi.org/10.1021/acsanm.0c01696.

[50] Y.Y. Xiong, J.Q. Li, L.L. Gong, X.F. Feng, L.N. Meng, L. Zhang, et al., Using mof-74 for hg2+ removal from ultra-low concentration aqueous solution, J. Solid State Chem. 246 (2017) 16–22, https://doi.org/10.1016/j.jssc.2016.10.018.

[51] S. Su, R. Zhang, J. Rao, J. Yu, X. Jiang, S. Wang, X. Yang, Fabrication of lanthanum-modified mof-808 for phosphate and arsenic(v) removal from wastewater, J. Environ. Chem. Eng. 10 (2022), 108527, https://doi.org/10.1016/j.jece.2022.108527.

[52] G.C. Shearer, S. Chavan, J. Ethiraj, J.G. Vitillo, S. Svelle, U. Olsbye, et al., Tuned to perfection: ironing out the defects in metal–organic framework uio-66, Chem. Mater. 26 (2014) 4068–4071, https://doi.org/10.1021/cm501859p.

[53] S. Mandal, M.K. Sahu, R.K. Patel, Adsorption studies of arsenic(iii) removal from water by zirconium polyacrylamide hybrid material (zrpacm-43), Water Resour. Ind. 4 (2013) 51–67, https://doi.org/10.1016/j.wri.2013.09.003.

[54] Z.-Q. Li, J.-C. Yang, K.-W. Sui, N. Yin, Facile synthesis of metal-organic framework mof-808 for arsenic removal, Mater. Lett. 160 (2015) 412–414, https://doi.org/10.1016/j.matlet.2015.08.004.

[55] L. Li, W. Ma, S. Shen, H. Huang, Y. Bai, H. Liu, A combined experimental and theoretical study on the extraction of uranium by amino-derived metal–organic frameworks through post-synthetic strategy, ACS Appl. Mater. Interfaces 8 (2016) 31032–31041, https://doi.org/10.1021/acsami.6b11332.

[56] P.V. Messina, P.C. Schulz, Adsorption of reactive dyes on titania–silica mesoporous materials, J. Colloid Interface Sci. 299 (2006) 305–320, https://doi.org/10.1016/j.jcis.2006.01.039.

[57] C. Namasivayam, R.T. Yamuna, Adsorption of direct red 12 b by biogas residual slurry: equilibrium and rate processes, Environ. Pollut. 89 (1995) 1–7, https://doi.org/10.1016/0269-7491(94)00056-J.